Thermomechanical modelling of the tribological surface transformations in the railroad network (white etching layer)

Léo Thiercelin, Loïc Saint-Aimé, Frédéric Lebon, Aurélien Saulot

Thermomechanical modelling of the tribological surface transformations in the railroad network (white eching layer)

Léo Thiercelin[a,b,c,*], Loïc Saint-Aimé[c], Frédéric Lebon[b], Aurélien Saulot[c]

[a] *IRT Railenium, F-59300, Famars, France*
[b] *Aix Marseille Univ, CNRS, Centrale Marseille, LMA UMR 7031, Marseille, France*
[c] *Univ. de Lyon, INSA-Lyon, UMR CNRS 5259 LaMCoS, F-69621, Villeurbanne, France*

Abstract

The formation of Tribological Surface Transformation (TST), known as white etching layer (WEL) in the wheel rail contact, corresponds to progressive and irreversible transformations on the surface of material due to the interaction of contact between two materials. The presence of WEL, damages the rails and cracks could initiate easily. Understanding the mechanisms of formation of WEL is important to prevent the problem of Rolling Contact Fatigue (RCF) in the rail network. The formation of the WEL is assumed to be due to a cyclic shear loading (at a high-frequency), under hydrostatic pressure associated with a moderate rise in temperature. Based on Transformed Induced Plasticity models and a previous model, a thermo-mechanical model taking into account the hydrostatic pressure, the shear stress and the temperature is presented to predict the formation of the WEL. An internal variable, representing all the steps of evolution of the microstructure leading to the WEL formation is introduced. 2-D finite element simulations of the rail running band (in the longitudinal direction) submitted to a cyclic thermomechanical loading are conducted to identify the model. The results are in good agreement with experimental observations for the size of the transformed zone after a given number of trains. The non-uniform repartition of WEL observed on the running band on trains could be

*Corresponding author
Email address: thiercelin@lma.cnrs-mrs.fr (Léo Thiercelin)

explained by local variations of the thermomechanical loading.

Keywords:
Rolling Contact Fatigue (RCF), White Etching Layer (WEL), Phase transformation, Tribological Surface Transformation (TST), Wheel/rail contact, Thermo-mechanical modelling

---

Nomenclature

λ, μ	Lame coefficients
α	Thermal expansion coefficient
σ^y	Classical yield strength
h	Linear isotropic hardening modulus
ξ, η	Characterisitc time of viscous effect associated with respectively the classical plasticity and the TRIP plasticity
κ	Parameter linked to the volumic change
T_0	Room temperature
T_i^z	Austenitization temperature
σ_c	Critical hydrostatic pressure
τ_c	Critical shear stress
ω_1	Parameter of sensitivity for the coupling between the temperature T and the hydrostatic pressure P
ω_2	Parameter of sensitivity for the coupling between the temperature T and the Von Mises equivalent stress σ^{eq}
ω_3	Parameter of sensitivity for the coupling between the hydrostatic pressure P and the Von Mises equivalent stress σ^{eq}

1. Introduction

Due to the increase of rail traffic combined with the rise of speed and loads of trains the rail network is subjected to the occurrence of many Rolling Contact Fatigue (RCF) defects such as squats. Squat defects damage the running band of the rail by the presence of cracks on the surface. In many studies, the squat

formation is correlated with the presence of Tribological Surface Transformations (TST) called the White Etching Layer (WEL) [1, 2, 3] for rail steel grades. Because of its brittleness and incompatibilities with the original material, cracks are observed in the vicinity of WEL either in the interface with the parent phase or within the WEL (Fig. 1).

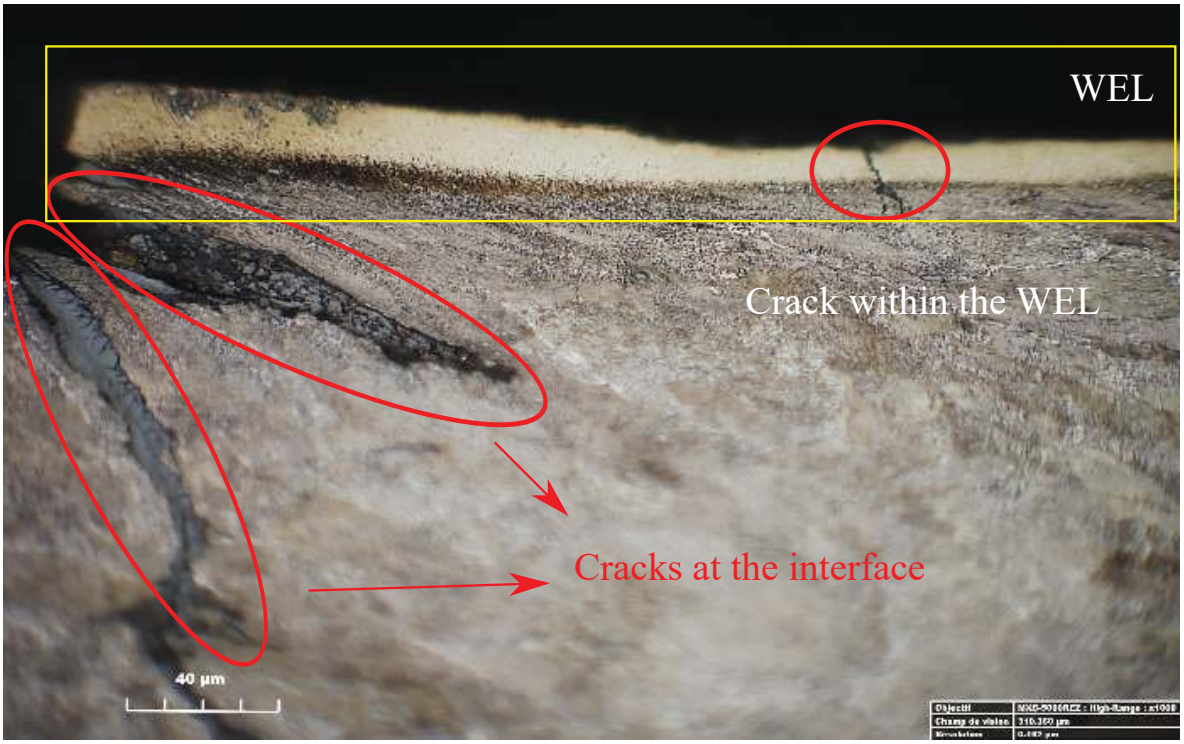

Figure 1: Longitudinal rail cross section in worn rail with the presence of cracks on the railroad after WEL formation at the WEL/pearlite interface and within the WEL

Understanding the mechanism of appearance and the nature of the WEL is then essential to prevent squat formation. Experimental studies have shown that the WEL is a solid-solid phase transformation of an initial pearlitic structure to either a martensitic or a "quasi-martensitic" structure (nano Fe-α grains saturated with C atom). Despite progress in techniques of analysis, the mechanism of WEL formation is still controversial. According to previous researches, WELs are the results of either mechanical [4, 5, 6, 7], thermal processes [1, 8, 9, 10] or a combination of both [11, 12, 13].

In some cases, due to its martensitic structure and the presence of retained austenite , the authors [1, 8, 9, 10, 12] deduced the WELs are induced by the

transformation of the pearlite into austenite followed by a rapid quenching transforming the austenite into the martensite. The presence of retained austenite would be due to an incomplete transformation. The austenitization of the steel is explained by an increase of a flash temperature above 700 °C (austenitization temperature). This temperature rise is generally attributed to friction in the contact zone in cases of braking or accelerating zone [4, 5] or after a grinding process [14]. Moreover, this could be due to the formation of Adiabatic Shear Bands (ASB) generated by an intense plastic deformation [1, 15]. According to Nakkalil [15], the WEL zones could be linked to a succession of ASBs that would join to form a homogenous layer. However, the contact temperature does not exceed 400 °C in normal condition [11, 16, 7, 17, 18]. In this mechanism the temperature is the driving force and the mechanical stresses facilitate the kinetics of transformation [19, 20, 21, 22].

Nevertheless, the retained austenite is not present in the whole WELs. Thus, another mechanism induced mechanically has been proposed to explain the formation of a nano Fe-α grains saturated with C atom [11, 6, 7, 2]. Indeed, in the case of cold drawing, Djaziri [23] proved the transformation of pearlite into martensite mechanically is possible without a prior austenitization. This mechanism is based on the severe plastic deformation that creates a high density of dislocations. The dislocations play a key role in the dissolution of cementite, the reduction of grain size and in the C migration [24, 25, 26]. In the case of the wheel/rail contact, the rail undergoes high repetitive contact stresses leading also to an accumulation of plastic deformation. The latter induces several microstructural changes until the WEL formation: cementite alignment with the rolling direction [27, 28], reduction of interlamellar spacing [29], breaking of cementite lamellaes and reduction of grain size [4, 5, 6, 7, 11]. All these steps will facilitate the cementite dissolution and the C migration [30]. In this mechanism the temperature is no longer the driving force of WEL formation but could catalyze the cementite dissolution and the C diffusion.

To summarize, the WEL transformation is induced by the accumulation of the train passage and has not a unique mechanism of formation. It depends on

the thermo-mechanical loadings history undergone by the running band of rails [13, 7].

Thus, a thermo-mechanical model is proposed to represent the progressive WEL formation whatever the mechanism of formation. The constitutive equations are mainly based on a previous model [31] that is reminded in the Section 2. Then, a description of the improvement of this model with a new yield surface of WEL formation is detailed in Section 3.

Thereafter, the model is implemented into a 2D Finite Element case representing the cumulative passage of trains. A study is done to estimate an order of magnitude of the parameters in wheel-rail contact conditions. Then a study of the variability of the thermomechanical field is realized to see how it could modify the kinetics of the WEL formation.

2. Thermo-mechanical model

In this section, we recall the thermomechanical model proposed by Antoni's works [31, 32]. Thus, all the state variables and all the equations given in this section were presented in Antoni's papers.

2.1. Motivations

As observed in the literature, the structure of WELs and their mechanism of formation differ from one study to another. However, from a macroscopic point of view, it is assumed that they have similar mechanical properties and they result from a cyclic thermo-mechanical process. Thus, the WEL formation will be considered as a progressive irreversible transformation of an initial pearlitic structure to a "martensitic-like" structure.

The modelling of the permanent solid–solid phase transformation induced mechanically was done in the past [33, 34, 35]. Those models concern materials that could transform from a parent phase to a daughter phase under mechanical stresses where the Von Mises stress is lower than the yield strength. It induces an abnormal plastic flow, called "TRansformed Induced Plasticity" (TRIP).

Using the assumption that the WEL results from a thermomechanical process and that there exists two kinds of plasticity in the process (classical isochoric plasticity and TRIP plasticity), a first phenomenological law of WEL formation was extended by Antoni [31].

2.2. State Variables

The state variables used in this model are divided into observable variables and internal variables.

Observable variables are the absolute temperature $T > 0$ and the total strain tensor $\boldsymbol{\epsilon}$ (with the assumption of small displacements). The strain tensor is decomposed into its spherical part $\frac{1}{3}\, Tr(\boldsymbol{\epsilon})\boldsymbol{G}$ and its deviatoric part $\boldsymbol{e}$ where $\boldsymbol{G}$ denotes the metric tensor (Eq. (1)).

$$\boldsymbol{\epsilon} = \frac{1}{3}\, Tr(\boldsymbol{\epsilon})\boldsymbol{G} + \boldsymbol{e} \tag{1}$$

Internal variables concern the variables associated with the classical isochoric plasticity and the TRIP plasticity.

For the classical isochoric plasticity, an isotropic hardening is assumed considering v as the isotropic hardening variable and $\boldsymbol{e^{pc}}$ the classical plastic deviatoric strain tensor.

For the TRIP plasticity, an internal variable z, ranging from 0 to 1, is defined. There are several interpretations of this variable from different points of view. From a metallurgical point of view, it corresponds to the proportion of a parent phase (pearlite) that has been transformed into a daughter phase (WEL). But this approach considers that the transformation is binary and that there exists an equilibrium between the two phases: the pearlitic structure (parent phase) and the WEL (daughter phase). However, the WEL formation is more complex and there are several steps to transform the original pearlite into WEL [30]. Thus z would be more likely an indicator of the different steps of transformation before obtaining the complete transformation. The gradient of the microstructure as observed in the works of Dylewski [29] can be correlated with

the gradient of the z value (Fig. 2). The closer z is to 1 the more the structure will approach a complete transformation into a WEL.

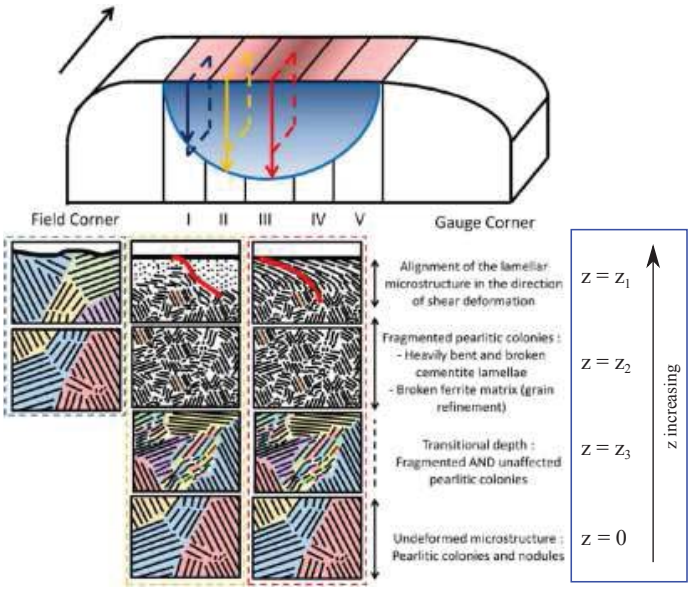

Figure 2: Schematic view of the tridimensional gradient of microstructure explained by Dylewski [29] interpreted numerically using an internal variable z (blue box)

The secondary variable denotes the TRIP plastic deviatoric strain tensor $\boldsymbol{e^{pz}}$ and corresponds to the plastic flow due to the phase transformation.

TRIP plasticity is accompanied by a density change ($\rho_{martensite} = 7800\ kg.m^{-3}$ and $\rho_{ferrite} = 7700\ kg.m^{-3}$). So, the total TRIP plastic strain tensor, $\boldsymbol{\epsilon^{pz}}$ is defined in Eq. (2). The parameter κ denotes the density change during the WEL formation.

$$\boldsymbol{\epsilon^{pz}} = \boldsymbol{e^{pz}} - \frac{1}{3}\frac{z}{\kappa}\boldsymbol{G} \tag{2}$$

2.3. Constitutive equations

The constitutive equations are described below:

$$\boldsymbol{\sigma} = -P\boldsymbol{G} + \boldsymbol{s} \tag{3}$$

$$P = -\frac{3\lambda + 2\mu}{3}\left(tr(\boldsymbol{\epsilon}) + \frac{z}{\kappa} - 3\alpha(T - T_0)\right) \tag{4}$$

$$\boldsymbol{s} = 2\mu(\boldsymbol{e} - \boldsymbol{e^{pc}} - \boldsymbol{e^{pz}}) \tag{5}$$

where $\boldsymbol{\sigma}$ is the Cauchy stress tensor, P is the hydrostatic pressure, $\boldsymbol{s}$ is the stress deviator tensor, (λ, μ) are the Lame coefficient, α the thermal expansion coefficient, T the absolute temperature and T_0 the room temperature.

The heat equation is given by:

$$\rho_i C_\epsilon \frac{T}{T_0}\dot{T} - k\Delta T = -(3\lambda+2\mu)\alpha T\, Tr(\dot{\boldsymbol{\epsilon}}) + \boldsymbol{s} : (\dot{\boldsymbol{e}}^{\boldsymbol{pc}} + \dot{\boldsymbol{e}}^{\boldsymbol{pz}}) - hv\dot{v} + \frac{1}{\kappa}[P - (3\lambda+2\mu)\alpha T]\dot{z} \tag{6}$$

where " Δ " is the Laplacian. The first term on the right hand side of Eq. (6) corresponds to thermo-elasticity, the second one, to TRIP-like plasticity and the classical plasticity and the last one, to the latent heat associated with the solid-solid phase transformation.

The equations of evolution of the internal state variables associated with the TRIP-like process (z and $\boldsymbol{e^{pz}}$) and the classical isochoric plasticity process (v and $\boldsymbol{e^{pc}}$) are detailed in the following sections.

2.4. Equations for the classical isochoric plasticity

Cyclic plasticity models for rail steel grades generally introduce a combination of kinematic and isotropic hardening to take into account the ratchetting response [36, 37, 38, 39]. It seems clear that the modelling of the WEL formation requires a cyclic plasticity model but the initial idea of this model was rather to focus on the modelling of the TRIP plasticity. Thus, for a first approach, a simple model of linear isotropic hardening is defined (where h is the linear isotropic modulus) in Eq. (7).

We consider a non-viscous plastic model. However, for the sake of numerical resolutions, this model is approached by a visco-plastic model which is regularized in order to converge to the non-viscous plastic model (Eq. 8 and 9). So, the parameter ξ is chosen small enough to tend towards the plasticity model. The plastic flow rate is oriented by the stress deviator tensor (Eq. (9)).

Yield function	$f^{pc}(\sigma^{eq}, v) = \sigma^{eq} - (\sigma^{y} + hv)$	(7)
Viscoplastic multiplier	$\dot{v} = \dfrac{< f^{pc}(\sigma^{eq}, v) >}{\xi \sigma^{y}}$	(8)
Flow rule	$\boldsymbol{\dot{e}^{pc}} = \dot{v} \dfrac{3}{2\sigma^{eq}} \boldsymbol{s}$	(9)

where σ^{eq} is the Von Mises equivalent stress, σ^{y} the classical yield strength, ξ is the characterisitc time of viscous effect associated with respectively the classical plasticity and the TRIP plasticity $< . >$ denotes the Macaulay brackets ($< x >= x$ when $x > 0$ and $< x >= 0$ when $x \leq 0$).

2.5. Equations for the TRIP plasticity

The expression of the yield function of the TRIP plasticity (Eq. (10)) is based on the assumption that the WEL transformation is induced by a coupling between a thermal term $f_{therm}(T)$ with a mechanical term $f_{meca}(P, \sigma^{eq})$. Whenever the difference between those two terms becomes positive, the WEL transformation is in progress which is numerically expressed by an evolution of the internal variable z. The choice of the formulation of the term $f_{meca}(P, \sigma^{eq})$ and its physical meaning are detailed in Section 3 (Eqs. (15) and (16)).

Again for the same reasons than the classical plasticity, the model of TRIP plasticity is approached by a visco-plastic model that is regularized. The parameter η must be chosen appropriately in order to converge towards a plastic model (Eq. 11). Similarly to the classical plasticity, the plastic flow rate linked to the WEL formation is also assumed to be oriented by the stress deviator tensor (Eq. (9)).

Yield function	$f^{pz}(P, \sigma^{eq}, T) = f_{therm}(T) - f_{meca}(P, \sigma^{eq})$	(10)
Viscoplastic multiplier	$\dot{p} = \dfrac{< 1 - z >}{\eta} < f^{pz}(P, \sigma^{eq}, T) > H(P)$	(11)
Flow rule 1	$\boldsymbol{\dot{e}^{pz}} = \dot{p} \dfrac{3}{2\sigma^{eq}} \boldsymbol{s};$	(12)
Flow rule 2	$\dot{z} = \kappa \dot{p}$	(13)

where $H(.)$ denotes the Heavyside step function ($H(x) = 1$ when $x \geq 0$ and $H(x) = 0$ when $x \leq 0$).

$f_{therm}(T)$ is a linear function of the temperature ranging from 0 to 1 for temperatures between the room temperature (T_0) and the critical temperature of transformation (T_i^z):

$$f_{therm}(T) = \frac{T - T_0}{T_i^z - T_0} \tag{14}$$

Remarks :

- Eq. (11) highlights the fact that phase transformation occurs only in a state of compression ($H(P) > 0$) and it ends once z reaches one ($< 1-z >$).
- Eq. (13) is consistent with the condition of the irreversibility of the transformation because $\dot{z}$ cannot be negative.

3. A phenomenological yield function of WEL formation

3.1. Formulation of the term $f_{meca}(P, \sigma^{eq})$ of the Eq. (10)

Numerous mechanical parameters may be responsible for the formation of WEL. The main factors that can be identified in the literature are the temperature, the hydrostatic pressure [21, 22, 40, 41], shear stresses [30, 41, 42] and the density of dislocations [6, 7, 24, 30]. Other authors have also suggested dynamic effects such as the rate of plastic deformation [15] or the frequency of stress [7].

The model developed by Antoni [31] allowed the qualitative prediction of WEL formation considering only a coupling between the hydrostatic pressure (P) and the temperature (T) (Eq. (15)). However, by interpolating the data from the literature [21, 22], the hydrostatic pressure reduces linearly the austenitization temperature by only 20 °C/GPa. Thus, under wheel/rail contact conditions (with a hydrostatic pressure in the order of 1 GPa), the austenitizing temperature will be reduced by about 20 °C. So it seems clear that the dependency of the hydrostatic pressure alone is insufficient to predict the WEL formation.

Therefore, a new formulation of the mechanical term f_{meca} based on the previous formulation is proposed taking into account a new variable associated with the deviatoric part of the stress tensor (Von Mises equivalent stress σ^{eq}) (Eq. (16) and (17)). Then, with this new model the WEL formation would result from a coupling between the hydrostatic pressure and the shear stress which is enhanced by the temperature.

$$f_{old} = f_{meca}(P) = e^{-\frac{<P>}{\omega_1}} \tag{15}$$

$$f_{new} = f_{meca}(P, \sigma^{eq}) = \frac{< e^{-\frac{<P>}{\omega_1}} - e^{-\frac{\sigma_c}{\omega_1}} >}{1 - e^{-\frac{\sigma_c}{\omega_1}}} \frac{< e^{-\frac{\sigma^{eq}}{\omega_2}} - e^{-\frac{\tilde{\tau}(P)}{\omega_2}} >}{1 - e^{-\frac{\tilde{\tau}(P)}{\omega_2}}} \tag{16}$$

With $\tilde{\tau}(P)$ defined as follow :

$$\tilde{\tau}(P) = \tau_c \frac{< e^{-\frac{<P>}{\omega_3}} - e^{-\frac{\sigma_c}{\omega_3}} >}{1 - e^{-\frac{\sigma_c}{\omega_3}}} \tag{17}$$

For the definition of the model, it is assumed that whatever the values of two variables, there is a value for the third one for which there is necessarily a phase transformation. In other words, it suggests the existence of three critical points:

- a critical temperature T_i^z
- a critical hydrostatic pressure σ_c
- a critical shear stress τ_c

The new yield function $f_{new}^{pz}(P, \sigma^{eq}, T)$ is then given as follow:

$$f_{new}^{pz}(P, \sigma^{eq}, T) = \frac{T - T_0}{T_i^z - T_0} - \frac{< e^{-\frac{<P>}{\omega_1}} - e^{-\frac{\sigma_c}{\omega_1}} >}{1 - e^{-\frac{\sigma_c}{\omega_1}}} \frac{< e^{-\frac{\sigma^{eq}}{\omega_2}} - e^{-\frac{\tilde{\tau}(P)}{\omega_2}} >}{1 - e^{-\frac{\tilde{\tau}(P)}{\omega_2}}} \tag{18}$$

This model takes well into account those critical points. Indeed, considering a thermo-mechanical state with $T = T_0$ and $\sigma^{eq} = 0$, the term f_{therm} is equal

to 0 and the new yield function f^{pz}_{new} will be then:

$$f^{pz}_{new}(P, \sigma^{eq} = 0, T = T_0) = -\frac{< e^{-\frac{<P>}{\omega_1}} - e^{-\frac{\sigma_c}{\omega_1}} >}{1 - e^{-\frac{\sigma_c}{\omega_1}}} \tag{19}$$

Thus, the only condition leading to a phase transformation will be when P exceeds σ_c. With the same reasoning, it is verified that τ_c and T^z_i are also critical transformation points with this formulation.

3.2. A 3-D representation

A parametric study of the new yield surface is presented in this section with the goal to develop a strategy to identify the parameters of the model. There are six parameters classified into two groups. The first one concerns the three critical points of transformation (T^z_i, σ_c and τ_c) and the other one is relative to three parameters of sensitivity for the coupling between the temperature, the hydrostatic pressure and the Von Mises equivalent stress (ω_1, ω_2 and ω_3).

A 3-D representation of the yield surface (with T, P and σ^{eq} as variables) is given by plotting the surface of equation $f^{pz}(T, P, \sigma^{eq}) = 0$ (Fig. 3).

It is possible to modify the curvature of the surface changing the value of one parameter of the parameters ω_i (Fig. 3). Each ω_i corresponds to the coupling between two variables separately so it is possible to identify them separately. A brief description of the process of identification is then given below.

The parameter ω_1 allows to modify the curvature of the surface in the plane pressure-temperature (Fig. 3). It could be identified by carrying out cyclic compression tests at various temperatures. It will give conditions of pressure and temperature leading to WEL formation or not. Thus, the suitable value of ω_1 will be the one that will modify correctly the curvature of the surface that delimits the conditions of the WEL formation.

The parameter ω_2 allows to modify the curvature of the surface in the plane shear stress-temperature (Fig. 3). It could be identified by carrying out cyclic shear tests at various temperatures.

Finally, The parameter ω_3 allows to modify the curvature of the surface in the plane shear stress-pressure (Fig. 3). It could be identified by conducting

cyclic shear tests under different hydrostatic pressure conditions.

If the coupling between the variable is unknown, for lack of experimental results, a linear coupling between the variables is possible taking ω_1, ω_2 and ω_3 high enough.

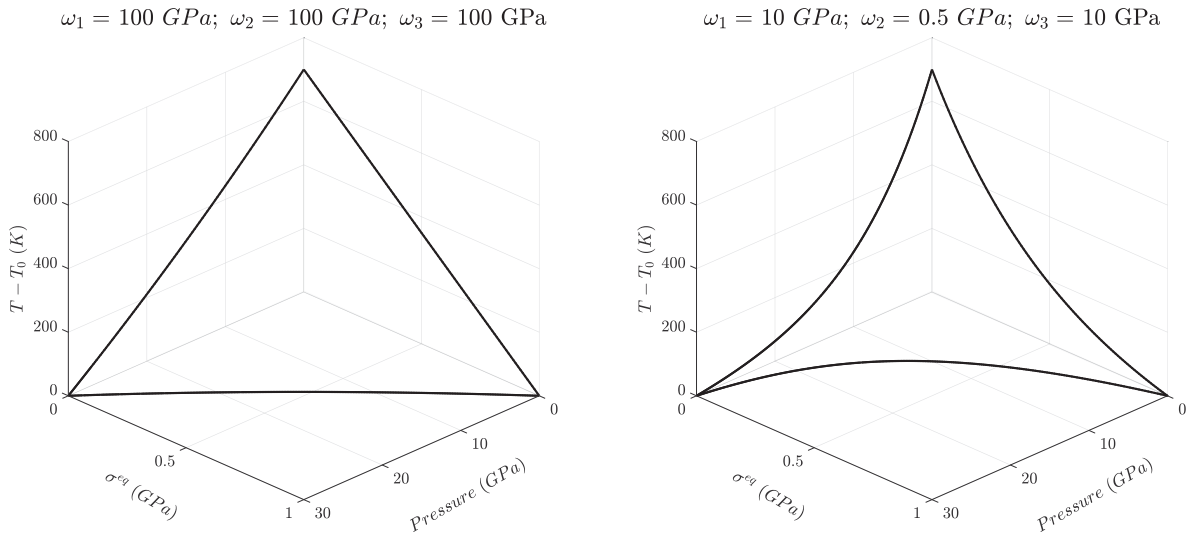

Figure 3: 3-D representation of the yield function $f^{pz}(P, \sigma^{eq}, T)$ and effects of the parameters of sensitivity ω_1, ω_2 and ω_3 on the curvature of the yield surface

Moreover, taking specific values of the parameters, it is possible to have a model independent of the stress σ^{eq} and to have an equivalent model of Antoni's model (see proof in Appendix). This model is then an extension of the previous one.

3.3. A methodology to identify the parameters of the model with the application of the wheel-rail contact

A first parametric study is made to identify and have an order of magnitude of each parameter in the case of the WEL formation in the wheel-rail contact. This methodology could be applied to any material presenting TSTs formation induced thermo-mechanically. The material modelled concerns a fully pearlitic steel (Carbon atome content of 0.77%) commonly used in the French Railway network (R260 steel grade [43]).

The first step is to identify the three critical points of transformation. The temperature of transformation noted T_i^z corresponds to the austenitization tem-

perature. In the case of the pearlitic steel, this temperature is equal to 722 °C (see Fe-C diagram under atmospheric pressure [22]). For the sake of simplicity, the temperature T_i^z is fixed to 1000 K.

Then, the litterature shows [21, 22] the austenitizing temperature decreases linearly with the hydrostatic pressure of around 20 °C/GPa. Thus, the coupling between the hydrostatic pressure and the temperature is considered as linear, ω_1 is thus arbitrarily chosen very high (100 GPa). Moreover, for the purpose of satisfying the hypothesis of a linear decrease of 20 °C/GPa, the hydrostatic pressure leading to a transformation at $T = T_0$ is assumed to be equal to $\sigma_c = 30\ GPa$.

The third critical point concerning the critical shear stress (τ_c) is unfortunately unknown in the literature but some studies showed the effect of the shear stress in facilitating the phase transformation [44]. A parametric study has to be done to see the sensitivity of this parameter on the yield surface.

At this stage, three parameters are identified (T_i^z, σ_c and ω_1) and will be fixed for the rest of the study (Table 1).

$T_i^z\ (K)$	$\sigma_c\ (GPa)$	$\omega_1\ (GPa)$
1000	30	100

Table 1: Parameters fixed for the rest of the study

Thus, a parametric study of the three other parameters (τ_c, ω_2 and ω_3) is made in the conditions of wheel-rail contact. In that case, the pressure is often around 1 GPa and the temperature in the contact could increase up to 300 °C in normal conditions (600 K). Thus, for the study, a contact pressure of 1 GPa and three temperatures (400 K, 500 K and 600 K) are then considered.

Dynamics contact conditions are experimentally difficult to estimate accurately, especially the tangential component in the real contact zone. Thus, the shear stress that could induce the WEL formation is unknown. So this model makes it possible to determine the critical shear stress $\sigma^{eq}_{critique}$ which will induce a phase transformation under different rail conditions. Therefore, with fixed

temperature and pressure, the yield function $f^{pz}_{new}(T, P, \sigma^{eq})$ is then a variable function depending of the shear stress. So, by plotting the mechanical term f_{new} with the shear stress it is possible to estimate this critical shear stress, i.e the shear stress such that f_{new} is so equal to the thermal term $f_{therm}(T)$. A parametric study on the parameters ω_2, ω_3 and τ_c is done to see their effect on the value of $\sigma^{eq}_{critique}$ (Fig. 4, 5 and 6).

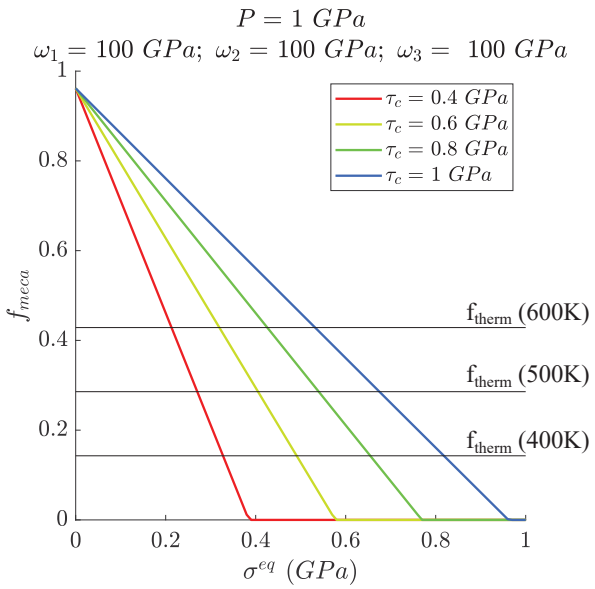

Figure 4: Effect of τ_c on the critical shear stress of transformation

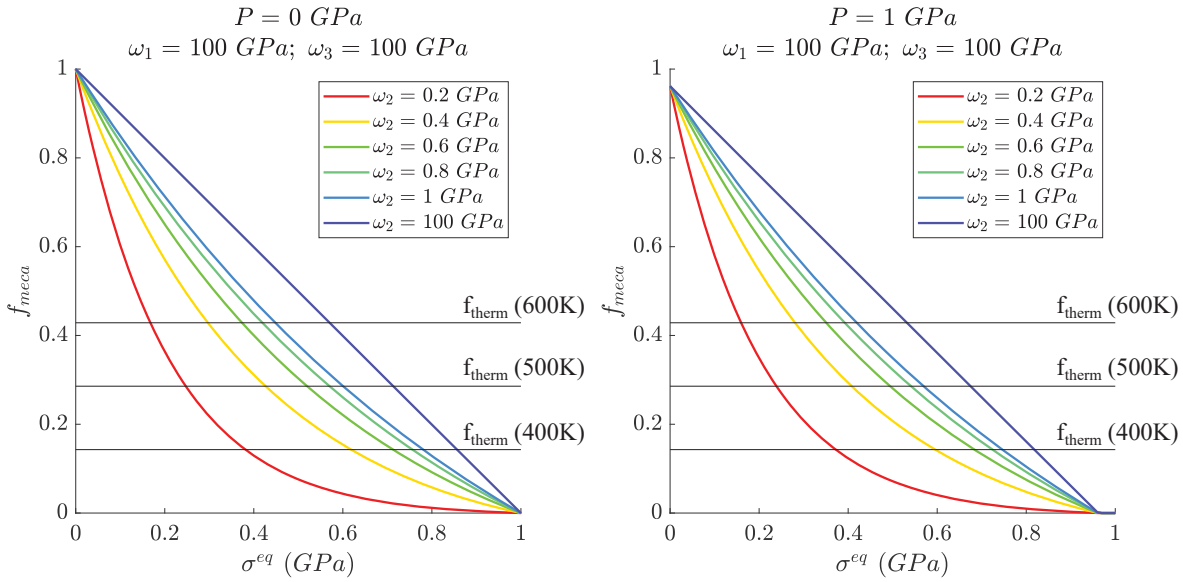

Figure 5: Effect of ω_2 on the critical shear stress of transformation

A general remark on the model is that whatever the values of the parameters,

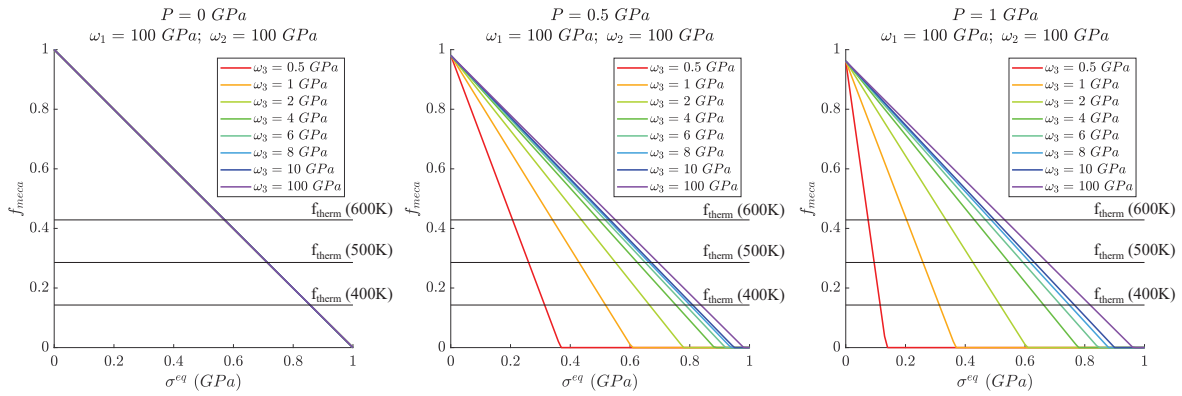

Figure 6: Effect of ω_3 on the critical shear stress of transformation

a rise in temperature and/or pressure will lower the value of $\sigma^{eq}_{critique}$, making the WEL formation easier to occur. So, the model is coherent with the assumption that the temperature and the pressure facilitate the WEL formation.

Concerning the parametric study, three Tables (Tables 2, 3 and 4) are presented to highlight the effect of each parameter. In fact, Table 2 reveals that the lower τ_c is, the lower $\sigma^{eq}_{critique}$ is. The same conclusion is done for ω_2 (Table 3) and ω_3 (Table 4), that denotes respectively the sensitivity of the coupling between the shear stress and the temperature (ω_2) and the coupling between the pressure and the shear stress (ω_3).

Therefore, ω_2, ω_3 and τ_c are three parameters that can modify the curvature (ω_2, ω_3) and the boundaries (τ_c) of the yield function $f^{pz}_{new}(T, P, \sigma^{eq})$. Moreover, they modifiy the value of the critical shear stress $\sigma^{eq}_{critique}$ necessary to induce the WEL formation. Thus, depending on the contact conditions, there could be WEL formation only if the shear stresses are higher than $\sigma^{eq}_{critique}$.

4. Wheel/rail contact problem (2D-Finite Element case)

4.1. Modelling of the wheel-rail contact

For this first study on a real case, simulations of a 2D model of the rail running band in the longitudinal direction submitted to a thermo-mechanical mobile field using the commercial FE software ABAQUS have been carried out (Figs. 7 and 8). The material behavior (Sections 2 and 3) has been implemented

$P\ (GPa)$	$T\ (K)$	$\omega_2\ (GPa)$	$\omega_3\ (GPa)$	$\tau_c\ (GPa)$	$\sigma^{eq}_{critique}\ (GPa)$
1	400	100	100	0.6	0.49
1	400	100	100	0.8	0.66
1	400	100	100	1	0.82
1	600	100	100	0.6	0.32
1	600	100	100	0.8	0.43
1	600	100	100	1	0.53

Table 2: Effect of τ_c on the critical shear stress $\sigma^{eq}_{critique}$

$P\ (GPa)$	$T\ (K)$	$\omega_2\ (GPa)$	$\omega_3\ (GPa)$	$\tau_c\ (GPa)$	$\sigma^{eq}_{critique}\ (GPa)$
1	400	0.2	100	1	0.37
1	400	0.6	100	1	0.68
1	400	1	100	1	0.75
1	600	0.2	100	1	0.16
1	600	0.6	100	1	0.35
1	600	1	100	1	0.42

Table 3: Effect of ω_2 on the critical shear stress $\sigma^{eq}_{critique}$

$P\ (GPa)$	$T\ (K)$	$\omega_2\ (GPa)$	$\omega_3\ (GPa)$	$\tau_c\ (GPa)$	$\sigma^{eq}_{critique}\ (GPa)$
0	300	$\forall\ \omega_2$	$\forall\ \omega_3$	1	$\tau_c = 1$
0.5	400	100	2	1	0.66
0.5	400	100	6	1	0.79
0.5	400	100	10	1	0.81
1	400	100	2	1	0.52
1	400	100	6	1	0.72
1	400	1	10	1	0.77

Table 4: Effect of ω_3 on the critical shear stress $\sigma^{eq}_{critique}$

as a user material subroutines (UMAT). The resolution of a thermomechanical problem is costly in terms of computational time especially if the thermal and

the mechanical problem are coupled. In order to reduce the computation time, a stationary resolution is chosen for the thermal problem. Thus, the two problems are uncoupled into a thermal problem that determines the temperature fields that will feed the mechanical problem.

For the calculation, a square (with a length of 100 mm) modelling the rail-head of the rail in the longitudinal direction in 2D is considered (Fig. 7). The mesh size is refined from the surface to five millimeters (that corresponds to the depth where the Von Mises stress is maximum in the rail [18]) with the smallest element size of 10 μm (Fig. 8). The mesh size has been so refined to satisfy the mesh convergence and to have the local thermo-mechanical state in the vicinity of the surface in order to be able to reproduce numerically the WEL formation in few dozen of microns from the surface (Fig 1).

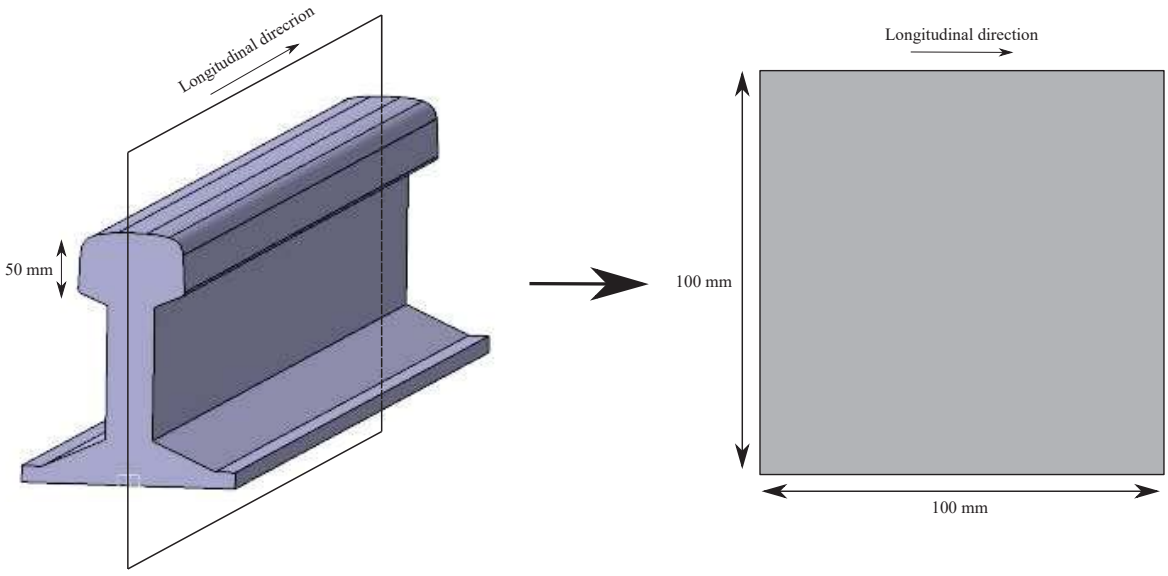

Figure 7: 3D model of the rail and the longitudinal model considered for the study

During a train passage, the rails undergoes severe and dynamic loads due to the wheel/rail contact interactions and to the dynamic of the train. The goal of the study is not to model accurateley the cyclic loading undergone by the rail but rather to have a simple case study. The latter must show the ability of the thermomecanical model to explain numerically with physical considerations the WEL formation in the surface of the rail.

A thermo-mechanical field that represents the passage of a wheel of a train

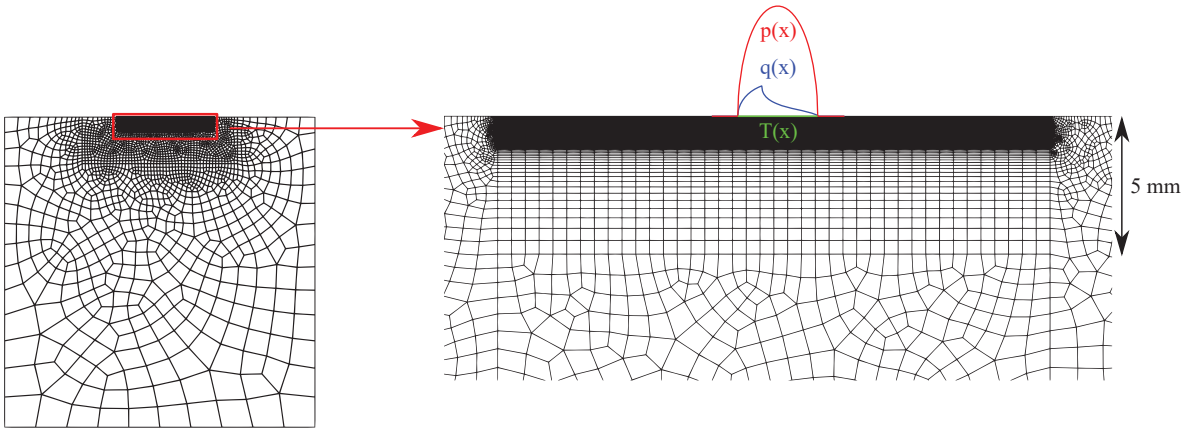

Figure 8: FE model of the rail (2D) with the thermo-mechanical field

is then applied to the rail surface. This field is composed of two mechanical fields (along normal and tangentiel directions) and a thermal field (Fig. 8). The normal mechanical field $p(x)$, which follows a theoretical Hertz profile, represents the pressure field exerted by the wheel on the rail (Eq. (20)). In 2D, the wheel-rail contact is considered lineic with a size of 2a. In real conditions, the contact zone changes because of the plasticity of the material so the size of contact $(2a)$ and the pressure are not constant [45]. Nevertheless, for the calculations the size of contact and the maximal pressure (p_0) are considered constant as a first approach. The value of a is then fixed to 5 mm that corresponds to the initial conditions in an elastic case [18]. p_0 denotes the maximal pressure on the contact and is fixed to 1 GPa. The tangential mechanical field $q(x)$ is modelled by the Carter theory (Eq. (21)) that is a simple way to model the traction loading of the wheel-rail contact in a first approach (Fig. 9). This theory divides grossly the contact zones into two parts, an adhesion zone that corresponds to the front edge of the wheel and a sliding zone to the back of the wheel. The size of the sliding zone is difficult to evaluate and it depends on the global (wheel slippage on the rail inducing creepage [**?**]) and local contact conditions. For the calculation, conditions of rolling with sliding are imposed to represent local sliding during a wheel passage. The adhesion zone and the slipping zone are arbitrarily chosen to be the same size ($c = a/2$ and $d = a - c$).

The thermal field is modelled by a temperature field. The aim of this study

is not to focus on the heat flows induced in the wheel-rail contact but rather to have an idealized case of contact with a simplified thermal field. Thus, a temperature T(x) field is imposed on the contact zone and assumes a uniform temperature T_i in the surface (Eq. (22)). The temperature is of the order of 450 K [16].

$$p(x) = p_0 \sqrt{1 - \left(\frac{x - x_0}{a}\right)^2}, \ with \ x \in [x_0 - a, x_0 + a] \tag{20}$$

Where x is the longitudinal coordinate of the point on the rail, x_0 the coordinate of the point in the contact center.

$$\begin{cases} q(x) = q_1(x) + q_2(x) \\ q_1(x) = \mu_0 \, p(x) \ with \ x \in [x_0 - a, x_0 + a] \\ q_2(x) = -\frac{c}{a} \mu_0 \, p_0 \sqrt{1 - \left(\frac{x - x_0 - d}{c}\right)^2} \ with \ x \in [x_0 + 2c - a, x_0 + a] \end{cases} \tag{21}$$

$$T(x) = \begin{cases} T_i \ if \ x \in [x_0 - a, x_0 + a] \\ T_0 \ otherwise \end{cases} \tag{22}$$

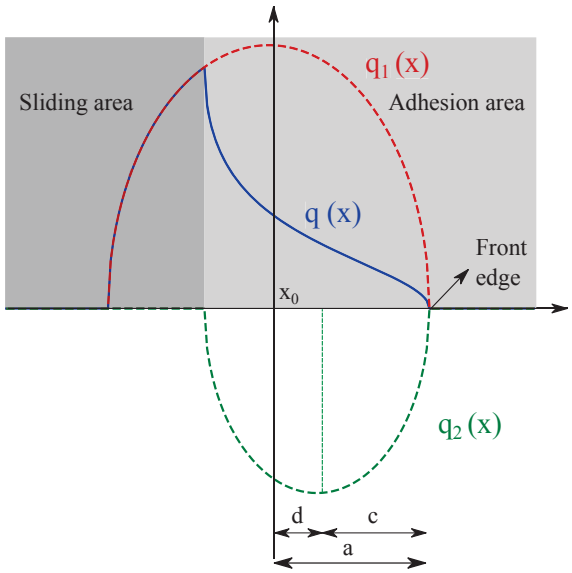

Figure 9: Carter field: x_0 is the center of the contact zone

The goal of this study is to be able to obtain results comparable to the observations of real rails. Based on the observations, three conditions are imposed in order to validate the model:

- Condition #1: In the classical thermomechanical conditions ($p_o = 1\ GPa$, $\mu_o = 0.3$, $T_i = 450\ K$), the transformed zone has a depth of less than 0.3 mm
- A variation of the thermomechanical conditions ($p_o + \Delta p$, $\mu_o + \Delta\mu$ and or $T_i + \Delta T$) increases the size of the transformed zone (called condition #2) and accelerates the kinetics of the WEL formation compared to classical conditions (called condition #3).

The first step is to see the influence of the missing parameters of the model (τ_c, ω_2 and ω_3) and the thermomechanical field (p_o, μ_o and T_i) on the size of the transformed zone. A first parametric study (τ_c, ω_2 and ω_3) after only one cycle is conducted with classical thermomechanical conditions (p_o, μ_o and T_i). After this step, by chosing a good set of parameters the condition #1 will be validated. Then, using this set of parameters, a study of the sensitivity of thermomechanical fields variations ($p_o + \Delta p$, $\mu_o + \Delta\mu$ and or $T_i + \Delta T$) is realized to validate the condition #2).

The second step consists in applying a cycling thermomechanical loading in order to see the effects of the last missing parameter (κ) and the thermomechanical fields variations on the kinetics of the WEL formation (condition #3).

4.2. Study for a first cycle

4.2.1. Parametric study of the parameters of the model

The parametric study of the model (τ_c, ω_2 and ω_3) is done in the classical thermomechanical conditions (p_o, μ_o and T_i). The study is carried out independently for each of the three parameters (τ_c, ω_2 and ω_3) by fixing the two latter (Fig. 10, 11 and 12). One thermomechanical cycle is applied and corresponds to one wheel pass.

To evaluate the effect of the parameter τ_c, defined as the critical shear stress, a linear coupling is defined, between the shear stress and the temperature on one hand ($\omega_2 = 100\ GPa = +\infty$) and between the shear stress and the hydrostatic pressure on the other hand ($\omega_3 = 100\ GPa = +\infty$). The higher τ_c is, the lower is the depth of the transformed zone. Indeed, by choosing a value of τ_c equal to 0.7 GPa the depth is of the transformed zone is of 3.3 mm whereas for a value of 0.75 GPa the depth is reduced to 0.3 mm (Fig. 10).

The study of the coupling between the shear stress and the temperature is now done (effect of ω_2). For this study, τ_c is now fixed to 1 GPa in order to have no significative influence of this parameter. A linear coupling between the shear stress and the pressure is once again considered ($\omega_3 = 100\ GPa$). The higher ω_2 is, the smaller is the depth of transformed zone. Indeed, by chosing a value of ω_2 equal to 0.4 GPa, the depth is 2 mm whereas for a value of 0.5 GPa the depth of the transformed zone is reduced to 0.5 mm (Fig. 11).

Similar conclusions are drawn concerning the coupling between the shear stresses and the hydrostatic pressure (effect of ω_3). In fact, the higher ω_3 is, the smaller the transformed zone is (Fig. 12).

At this stage, there is not a unique set of parameters leading to a transformed zone at most 0.3 mm thick under the classical thermomechanical conditions. Thus, the condition for obtaining a transformed zone of a maximimum thickness of 0.3 mm (condition #1) is satisfied for a multiple set of parameters. The best set of parameters will depend on the sensitivity of each coupling that has to be fed experimentally with dedicated shear test under pressure and temperature controlled (work in progress for a future paper). Because of the lack of experimental data available at this time, an arbitrary set of parameters verifiying the condition #1 is considered and will be fixed for the rest of the study (Table 5).

$\tau_c\ (GPa)$	$\omega_2\ (GPa)$	$\omega_3\ (GPa)$
1	100	4

Table 5: Parameters chosen for the WEL model

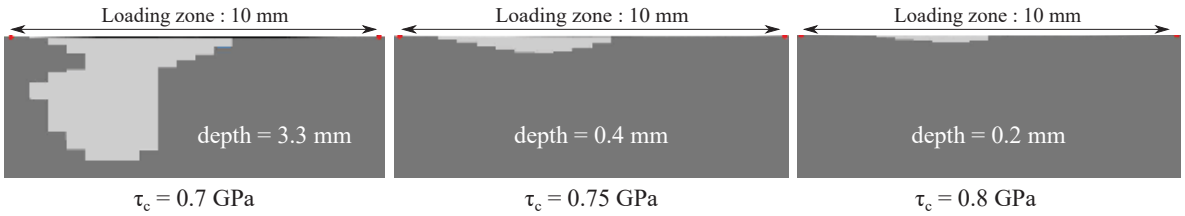

Figure 10: Effect of τ_c on the depth of the transformed area (with $\omega_2 = \omega_3 = 100\,GPa$)

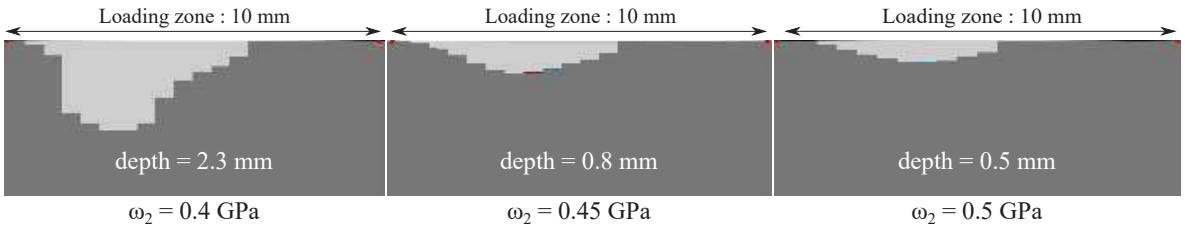

Figure 11: Effect of ω_2 on the depth of the transformed area (with $\tau_c = 1\ GPa$ and $\omega_3 = 100\ GPa$)

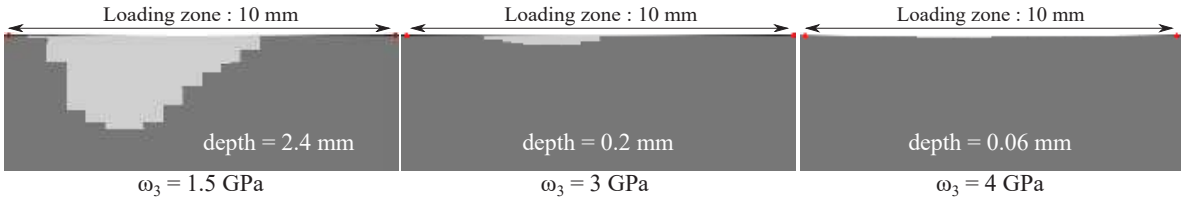

Figure 12: Effect of ω_3 on the depth of the transformed area (with $\tau_c = 1\ GPa$ and $\omega_2 = 100\ GPa$)

4.2.2. Effects of the variability of the thermomechanical fields

During a train passage, the rail undergoes a cyclic thermomechanical field that is not constant. There are three main variations that are summurized below:

- A variation of the normal forces [46, 47, 48, 49, 50]: those variations are due to two scales of the contact, from a macroscopic point of view (multibody dynamics, infrastructure) and at the microscale (imperfection of contact, rugosity, corrugation). For this first study, those variations will simply be modelled by a variation of the maximal Hertz pressure ($p_o + \Delta p$).
- A variation of the tangential forces [51, 52, 53, 54]: the tangential forces are often unknown because they depend on the contact conditions that could change with many factors (adhesion, rugosity, climate factors, third

body). The effect of the variation will be numerically driven by a variation of the coefficient of friction ($\mu_o + \Delta\mu$).

- A temperature variation [1, 16, 55, 17, 15]: the temperature change is due to frictional power dissipation, the plasticity and also, in some specific cases, from electrical breakdown. Depending on the contact conditions, in particular the sliding part there could be a variation of the heat flow and thus variations of the temperature. The change of temperature will then be a variation of the surface temperature imposed ($T_i + \Delta T$).

A parametric study is conducted to see the effect of the variability of the thermomechanical loading on the depth of the transformed zone. Whatever the increase of one of those variables, the thickness of the transformed zone increases (Fig. 13, 14 and 15). The second observation is that when simultaneous variations of several variables are applied, the thickness of the transformed zone increases a lot more than when there is a unique variation (Fig. 16). Thus, local variations of the thermomechanical variables could lead to WEL patches with non uniform size which is exactly what is observed on the worn rails, the condition #2 is thus verified. The next step is to pursue the analysis by now applying cyclic loading to model the progressive WEL formation after a given number of trains.

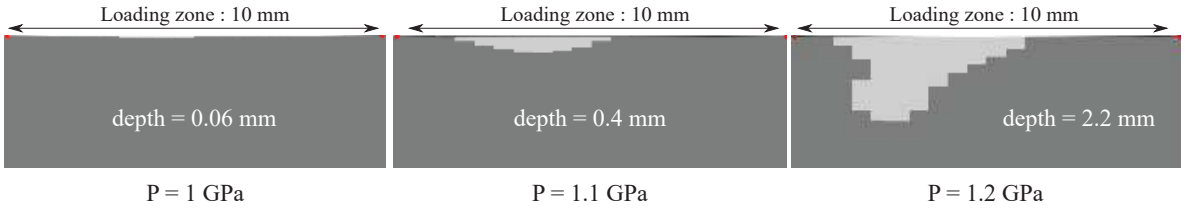

Figure 13: Effect of the contact pressure on the transformed zone (with $\mu_o = 0.3$ and $T_i = 450\ K$)

4.3. Study for cyclic loading

The goal of this section is to determine the number of train producing a WEL zone (quasi complete transformation when the internal variable z is equal

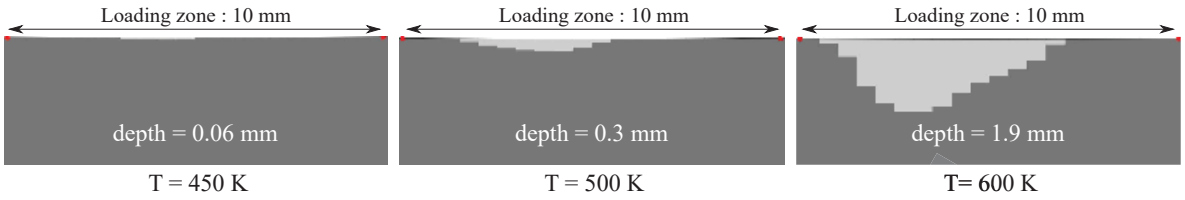

Figure 14: Effect of the temperature on the transformed zone (with $P_o = 1\ GPa$ and $\mu_o = 0.3$)

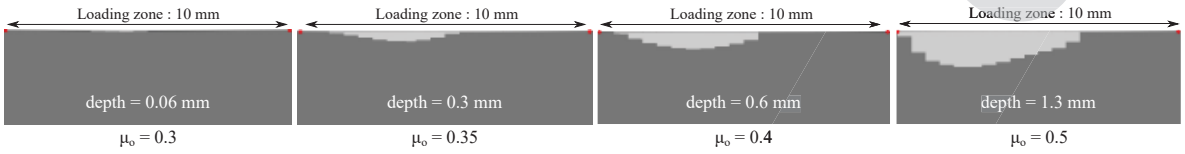

Figure 15: Effect of the coefficient of friction on the transformed zone (with $P_o = 1\ GPa$ and $T_i = 450\ K$)

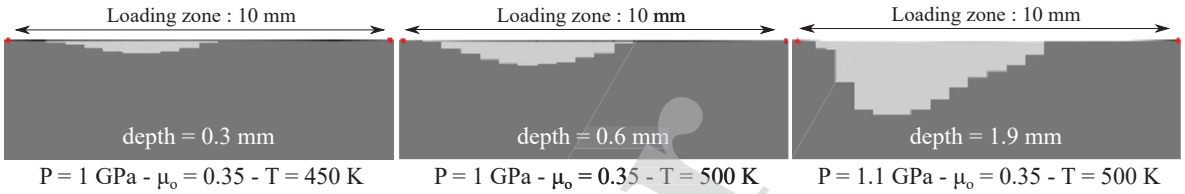

Figure 16: Effect of simultaneous variations of the thermomechanical variables (1, 2 or 3) on the transformed zone

to 0.95) with a depth of less than 0.1 mm. A cyclic thermo-mechanical loading is applied at the coordinate x_0. The period of the cyclic loading, representing the contact time for one wheel passage is fixed at $4.10^{-4}\ s$ [6]. Knowing that a high-speed train ("TGV" in the French Rail network) is composed of 15 bogies (thus 30 axles), a train passage is assumed to correspond to 30 cycles in the computations.

A map of the internal variable z field is presented in the Figure 17 after 100 trains pass under classical contact conditions with a coefficient of friction of 0.4 ($p_o = 1\ GPa$, $\mu_o = 0.4$ and $T_i = 450\ K$). A gradient of the z variable is denoted and could be successfully correlated with the gradient of the microstructure change observed in the worn rails [29] (Fig. 2). Moreover, a few dozen microns from the surface, the value of z exceeds 0.95, which reflects a quasi-complete WEL transformation in the vicinity of the surface. The shape and the size of the numerical WEL zone are consistent with the WEL patches on the railroads

(Fig. 1). Thus, this model can qualitatively and physically reproduce the WEL formation induced by a train passage accumulation.

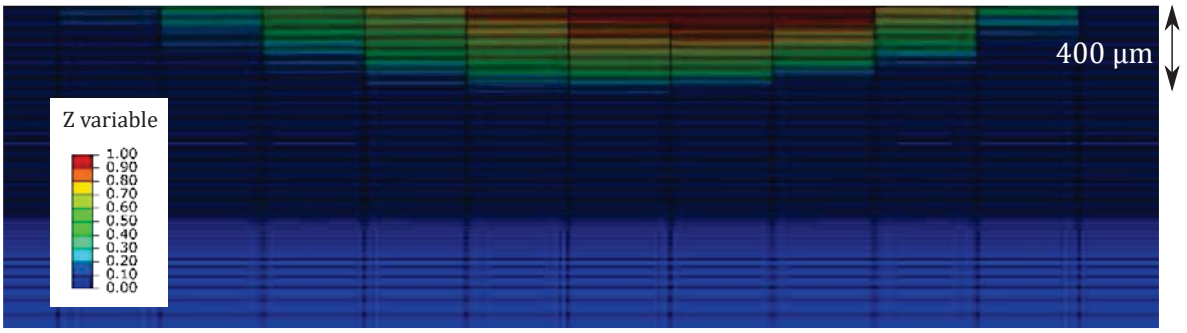

Figure 17: Example of the gradient of transformed zone after 100 trains : $P_o = 1\ GPa$, $\mu_o = 0.4$ and $T_i = 450K$

A parametric study of the kinetics of the z variable is subsequently carried out to see the effect of the parameter κ and the effect of the variations of the thermomechanical field (Eq. (12) and (13)).

The study of sensitivity to the parameter κ shows that the higher κ is, the faster is the transformation (Fig. 18). Indeed, for a value of κ equal to 200, the number of trains needed to reach a quasi complete transformation is around 90 whereas for $\kappa = 300$, the number of trains is reduced to 70.

Then, variations of the thermochanical loading (Δp, $\Delta \mu$ or ΔT) are considered to see their effects on the kinetics of z and the number of trains necessary to obtain a quasi complete WEL transformation with a thickness of a few dozen microns.

Whatever the increase of one of those variables (Δp, $\Delta \mu$ or ΔT), the WEL transformation is faster than in the classical conditions (Fig. 19, 20, 21 and 22). For example, an increase of 10% of the pressure will decrease the number of the train necessary to have a complete WEL transformation (Fig. 19). Moreover, a combination of simultaneous variations will accelerate the kinetics of WEL formation (Fig. 22).

The second striking feature is that a variation of different variables could lead to both the same kinetics and the same number of trains leading to complete WEL transformation. Indeed, considering an increase of the coefficient of

friction from 0.3 to 0.4 or an increase of the pressure from 1 GPa to 1.2 GPa, 60 trains are required to reach a quasi complete transformation (Fig. 23). In addition, a simultaneous combination of several variations can also lead to the same number of trains ($p = 1.1\ GPa$, $\mu = 0.35$ and $T = 450\ K$) (Fig. 23). The path to obtain a plain WEL is not unique.

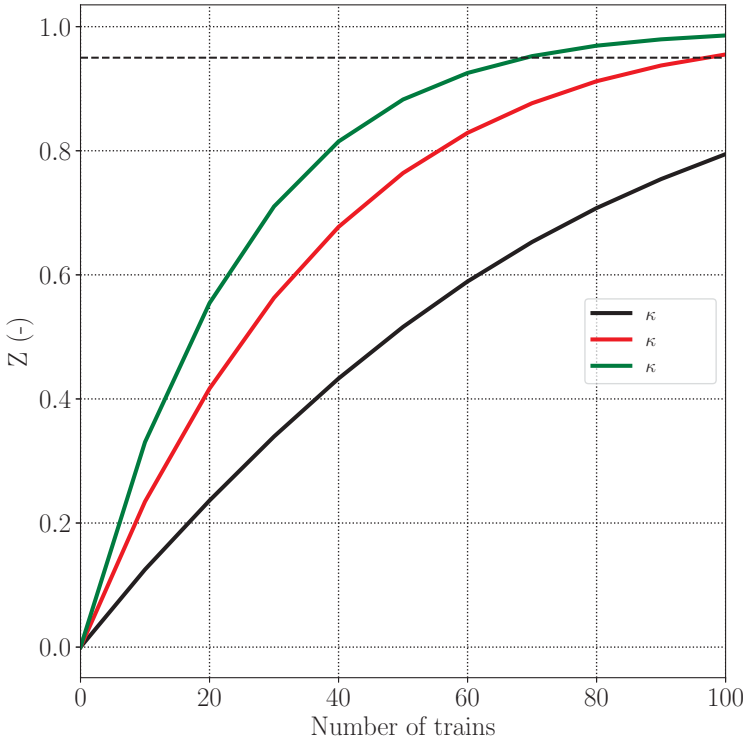

Figure 18: Effect of κ on the kinetics of the z variable

5. Conclusion

A thermomechanical model of the WEL formation has been implemented as an improvement of a previous model. This model considers that the WEL formation results from repetitive thermomechanical loadings.

An internal variable, z, is introduced to model the microstructural evolutions leading to the formation of WEL. The kinetics of this variable is controlled by a coupling between shear stresses, hydrostatic pressure and temperature (Eq. 16).

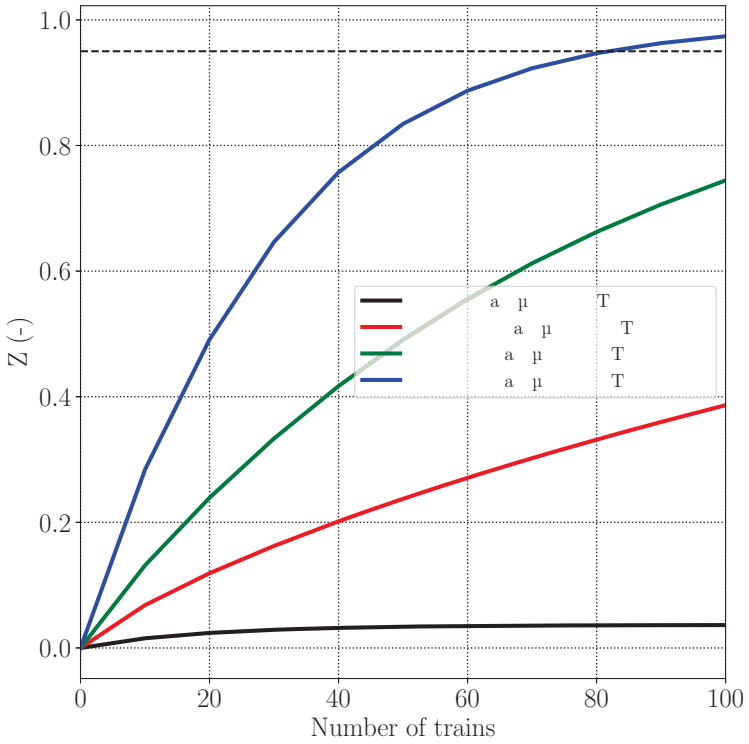

Figure 19: Effect of the variability of the pressure on the kinetics of the z variable

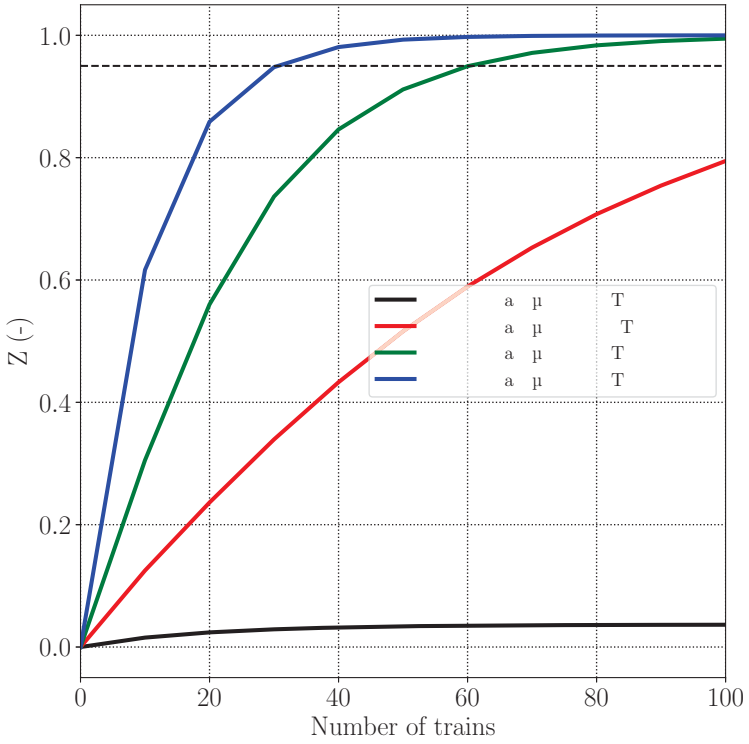

Figure 20: Effect of the variability of the coefficient of friction on the kinetics of the z variable

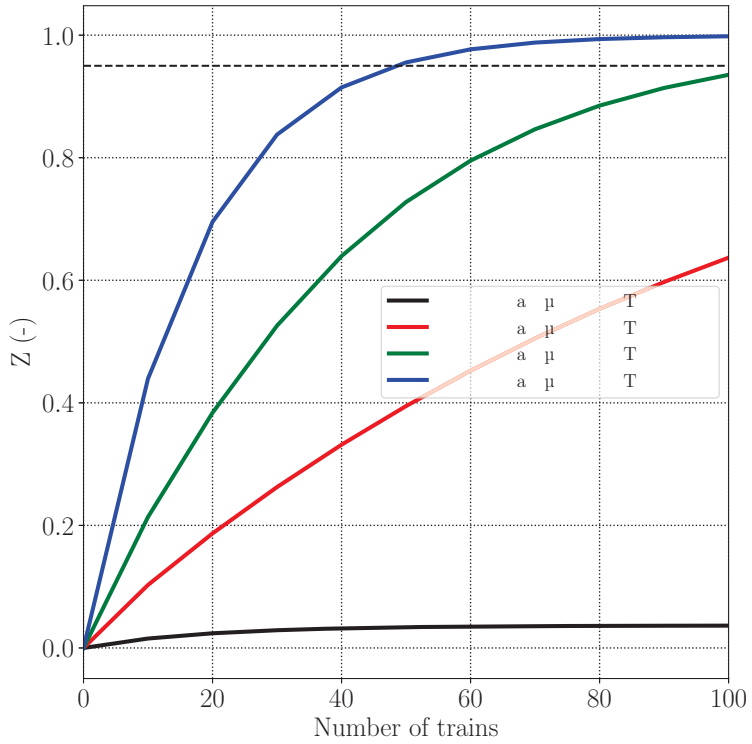

Figure 21: Effect of the variability of the temperature on the kinetics of the z variable

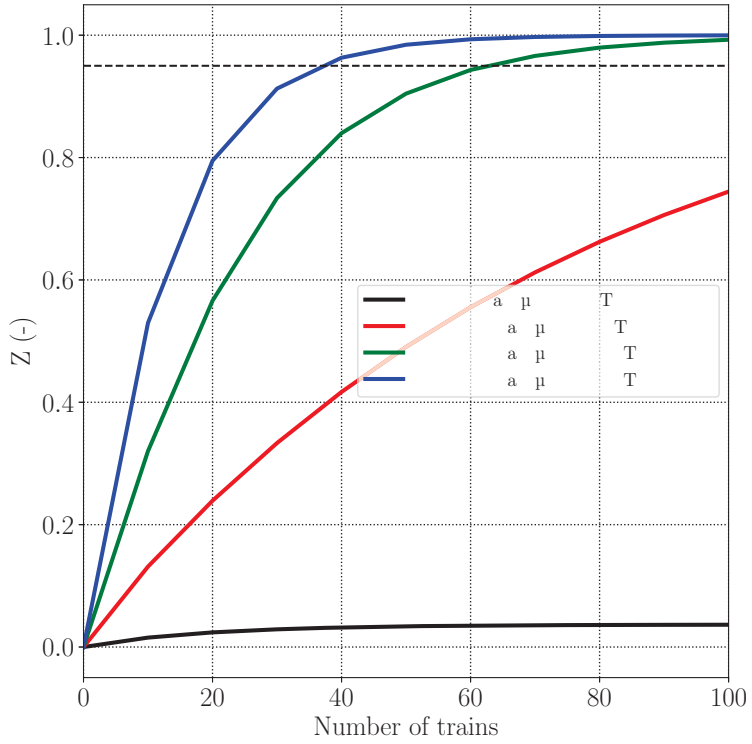

Figure 22: Effect of the variations of several variables on the kinetics of the z variable

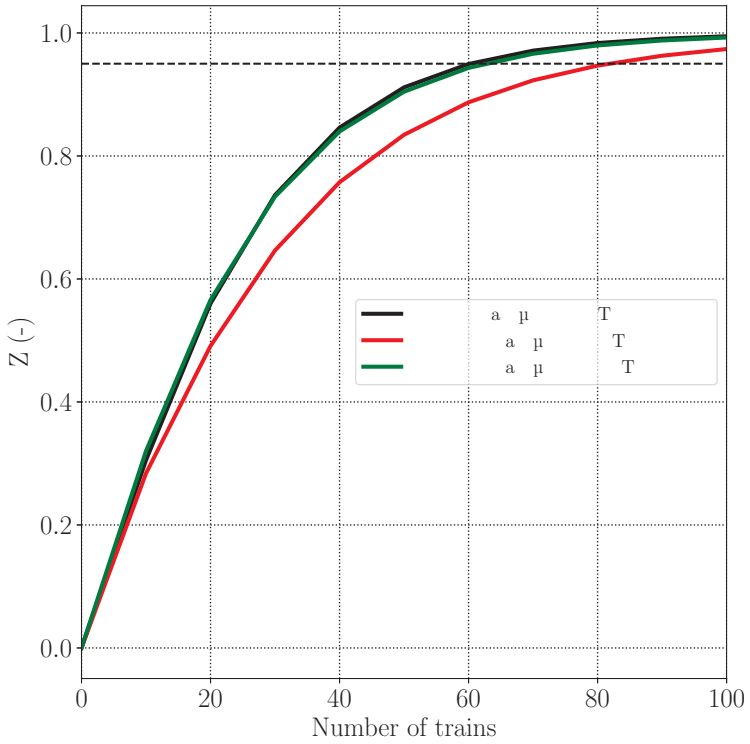

Figure 23: Similar kinetics obtained considering different variations of the thermomechanical fields

Using the example of the WEL formation in the railroad, a numerical methodology to identify all the parameters of the model was developed. This new model is able to give a physically better prediction of the WEL formation than the previous one [31]. It takes into account the dependency of the thermomechanical loading and the accumulation of trains. Indeed, it predicts qualitatively the depth of the transformed zone (in agreement with microstructural observations) and with a simple kinetics law, it can also estimate the number of trains leading to the WEL formation.

In addition, this model helps to explain the progressive formation of discontinuous WEL patches on the rail surface that could be attributed to local and dynamical variations of the thermomechanical loads (local changes in contact pressures, tangential forces and temperature). Those variations change the kinetics of the z variable and thus could lead to a sparse repartition of WEL spots.

In order to represent more physically the behavior of the material, a more

complex model of the classical plasticity has to be done (model of cyclic plasticity using Chaboche model [39, 56]). Moreover, experiments will be done to identify more accurately the parameters of the model.

This model is a promising tool to better understand and anticipate the formation of WEL in the wheel/rail contact, depending on the thermomechanical conditions applied to the rail. From a broader point of view, this model could be applied to the formation of TST in other areas that would be associated with thermomechanical coupling.

Aknowledgments

This work is part of the multi-disciplinary project MOPHAB, which aims to improve knowledge and understanding of the mechanisms leading to the formation of White Etching Layer in the materials used to construct railways, and to develop numerical models. The authors would like to thank IRT Railenium for their funding support and the industrials partners for their support (RATP, SNCF, British Steel).

Appendix

Model independent of σ^{eq} - equivalence with the previous model

With this model, it is possible to neglect the shearing effect and to recover an expression of the previous model. To omit the shearing effect in the model, the following values of the parameters must be taken into account:

$$\begin{cases} \tau_c = +\infty \\ \omega_2 = +\infty \\ \tau_c \gg \omega_2 \end{cases} \tag{23}$$

The passage to the limit of the function $\tilde{\tau}(P)$ gives:

$$\lim_{\tau_c \to +\infty} \tilde{\tau}(P) = +\infty$$

The passage to the limit of the function $\tilde{\tau}(P)$ leads to: f^{pz} :

$$\lim_{\substack{\tau_c \to +\infty \\ \omega_2 \to +\infty \\ \tau_c \gg \omega_2}} \frac{< e^{-\frac{\sigma^{eq}}{\omega_2}} - e^{-\frac{\tilde{\tau}(P)}{\omega_2}} >}{1 - e^{-\frac{\tilde{\tau}(P)}{\omega_2}}} = \lim_{\omega_2 \to +\infty} e^{-\frac{\sigma^{eq}}{\omega_2}} = 1$$

Then the function $f_{meca}(P, \sigma^{eq}, T)$ can be simplified:

$$\lim_{\substack{\tau_c \to +\infty \\ \omega_2 \to +\infty \\ \tau_c \gg \omega_2}} f_{new} = \frac{< e^{-\frac{<P>}{\omega_1}} - e^{-\frac{\sigma_c}{\omega_1}} >}{1 - e^{-\frac{\sigma_c}{\omega_1}}}$$

The yield function is then:

$$f^{pz}_{new}(P, \sigma^{eq}, T) = \tilde{f}^{pz}_{new}(P, T) = \frac{T - T_0}{T_i^z - T_0} - \frac{< e^{-\frac{<P>}{\omega_1}} - e^{-\frac{\sigma_c}{\omega_1}} >}{1 - e^{-\frac{\sigma_c}{\omega_1}}} \tag{24}$$

With the parameters τ_c and ω_2 taken large enough a model depending only on the temperature and the hydrostatic pressure is obtained. Only two parameters are to be identified in this case: σ_c and ω_1.

By taking a particular value of the parameter σ_c (Eq. 25) an equivalent expression of the Antoni's yield surface is obtained (proof below).

$$\sigma_c = \omega_1 \ln \left(\frac{T_i^z}{T_0} \right) \tag{25}$$

Proof ($P < \sigma_c$):

$$\tilde{f}^{pz}_{new}(P, T) = \frac{T - T_0}{T_i^z - T_0} - \frac{< e^{-\frac{<P>}{\omega_1}} - e^{-\frac{\sigma_c}{\omega_1}} >}{1 - e^{-\frac{\sigma_c}{\omega_1}}}$$

$$\tilde{f}^{pz}_{new}(P, T) = \frac{T - T_0}{T_i^z - T_0} - \frac{e^{-\frac{<P>}{\omega_1}} - \frac{T_0}{T_i^z}}{1 - \frac{T_0}{T_i^z}}$$

$$\tilde{f}^{pz}_{new}(P, T) = \frac{\frac{T}{T_i^z} - \frac{T_0}{T_i^z}}{1 - \frac{T_0}{T_i^z}} - \frac{e^{-\frac{<P>}{\omega_1}} - \frac{T_0}{T_i^z}}{1 - \frac{T_0}{T_i^z}}$$

$$\tilde{f}^{pz}_{new}(P, T) = \frac{T_i^z}{T_i^z - T_0} f^{pz}_{old}(P, T) \tag{26}$$

References

[1] W. Daniel, Final Report on the Rail Squat Project R3-105, Final Report on the Rail Squat Project R3-105, CRC for rail innovation, Australia, 2013.

[2] S. Simon, A. Saulot, C. Dayot, X. Quost, Y. Berthier, Tribological characterization of rail squat defects, Wear 297 (2013) 926–942.

[3] M. Steenbergen, R. Dollevoet, On the mechanism of squat formation on train rails – Part I: Origination, International Journal of Fatigue 47 (2013) 361–372.

[4] A. Al-Juboori, D. Wexler, H. Li, H. Zhu, C. Lu, A. McCusker, J. McLeod, S. Pannil, Z. Wang, Squat formation and the occurrence of two distinct classes of white etching layer on the surface of rail steel, International Journal of Fatigue 104 (2017) 52–60.

[5] A. Al-Juboori, H. Zhu, D. Wexler, H. Li, C. Lu, A. McCusker, J. McLeod, S. Pannila, J. Barnes, Characterisation of White Etching Layers formed on rails subjected to different traffic conditions, Wear 436-437 (2019) 202998.

[6] W. Lojkowski, M. Djahanbakhsh, G. Bürkle, S. Gierlotka, W. Zielinski, H.-J. Fecht, Nanostructure formation on the surface of railway tracks, Materials Science and Engineering: A 303 (2001) 197–208.

[7] S. Newcomb, W. Stobbs, A transmission electron microscopy study of the white-etching layer on a rail head, Materials Science and Engineering 66 (1984) 195–204.

[8] W. Österle, H. Rooch, A. Pyzalla, L. Wang, Investigation of white etching layers on rails by optical microscopy, electron microscopy, X-ray and synchrotron X-ray diffraction, Materials Science and Engineering: A 303 (2001) 150–157.

[9] J. Takahashi, K. Kawakami, M. Ueda, Atom probe tomography analysis of the white etching layer in a rail track surface, Acta Materialia 58 (2010) 3602–3612.

[10] L. Wang, A. Pyzalla, W. Stadlbauer, E. Werner, Microstructure features on rolling surfaces of railway rails subjected to heavy loading, Materials Science and Engineering: A 359 (2003) 31–43.

[11] G. Baumann, K. Knothe, H.-J. Fecht, Surface modification, corrugation and nanostructure formation of high speed railway tracks, Nanostructured Materials 9 (1997) 751–754.

[12] J. Wu, R. Petrov, S. Kölling, P. Koenraad, L. Malet, S. Godet, J. Sietsma, Micro and Nanoscale Characterization of Complex Multilayer-Structured White Etching Layer in Rails, Metals 8 (2018) 749.

[13] A. Kumar, G. Agarwal, R. Petrov, S. Goto, J. Sietsma, M. Herbig, Microstructural evolution of white and brown etching layers in pearlitic rail steels, Acta Materialia 171 (2019) 48–64.

[14] C. J. Rasmussen, S. Fæster, S. Dhar, J. V. Quaade, M. Bini, H. K. Danielsen, Surface crack formation on rails at grinding induced martensite white etching layers, Wear 384-385 (2017) 8–14.

[15] R. Nakkalil, Formation of adiabatic shear bands in eutectoid steels in high strain rate compression, Acta Metallurgica et Materialia 39 (1991) 2553–2563.

[16] M. Ertz, K. Knothe, A comparison of analytical and numerical methods for the calculation of temperatures in wheel-rail contact (2002) 11.

[17] V. Linck, A. Saulot, L. Baillet, Consequence of contact local kinematics of sliding bodies on the surface temperatures generated, Tribology International 39 (2006) 1664–1673.

[18] P. T. Zwierczyk, Thermal and Stress Analysis of a Railway Wheel-Rail Rolling-Sliding Contact, PhD, Budapest University of Technology and Economics, Budapest, 2015.

[19] G. Baumann, H. Fecht, S. Liebelt, Formation of white-etching layers on rail treads, Wear 191 (1996) 133–140.

[20] A. Al-Juboori, H. Zhu, D. Wexler, H. Li, C. Lu, A. McCusker, J. McLeod, S. Pannila, J. Barnes, Evolution of rail surface degradation in the tunnel: The role of water on squat growth under service conditions, Engineering Fracture Mechanics 209 (2019) 32–47.

[21] J. E. Hilliard, Iron-carbon phase diagram isobaric sections of the eutectoid region at 35, 50 and 65 kilobars., Transactions of the Metallurgical Society of AIME 227 (1963) 429–438.

[22] J. Wu, R. H. Petrov, M. Naeimi, Z. Li, R. Dollevoet, J. Sietsma, Laboratory simulation of martensite formation of white etching layer in rail steel, International Journal of Fatigue 91 (2016) 11–20.

[23] S. Djaziri, Y. Li, G. A. Nematollahi, B. Grabowski, S. Goto, C. Kirchlechner, A. Kostka, S. Doyle, J. Neugebauer, D. Raabe, G. Dehm, Deformation-Induced Martensite: A New Paradigm for Exceptional Steels, Advanced Materials 28 (2016) 7753–7757.

[24] V. Gavriljuk, Decomposition of cementite in pearlitic steel due to plastic deformation, Materials Science and Engineering: A 345 (2003) 81–89.

[25] J. Languillaume, G. Kapelski, B. Baudelet, Cementite dissolution in heavily cold drawn pearlitic steel wires, Acta Materialia 45 (1997) 1201–1212.

[26] X. Sauvage, J. Copreaux, F. Danoix, D. Blavette, Atomic-scale observation and modelling of cementite dissolution in heavily deformed pearlitic steels, Philosophical Magazine A 80 (2000) 781–796.

[27] F. Alwahdi, A. Kapoor, F. Franklin, Subsurface microstructural analysis and mechanical properties of pearlitic rail steels in service, Wear 302 (2013) 1453–1460.

[28] W. R. A. Tyfour, Interaction between Wear and Rolling Contact Fatigue in Pearlitic Rail Steels, Ph.D. thesis, University of Leicester, 1995.

[29] B. Dylewski, M. Risbet, S. Bouvier, The tridimensional gradient of microstructure in worn rails – Experimental characterization of plastic deformation accumulated by RCF, Wear 392-393 (2017) 50–59.

[30] Y. Ivanisenko, W. Lojkowski, R. Valiev, H.-J. Fecht, The mechanism of formation of nanostructure and dissolution of cementite in a pearlitic steel during high pressure torsion, Acta Materialia 51 (2003) 5555–5570.

[31] G. Antoni, T. Désoyer, F. Lebon, A combined thermo-mechanical model for Tribological Surface Transformations, Mechanics of Materials 49 (2012) 92–99.

[32] G. Antoni, F. Lebon, T. Désoyer, Return Mapping Algorithms (RMAs) for Two-Yield Surface Thermoviscoplastic Models Using the Consistent Tangent Operator, International Journal of Nonlinear Sciences and Numerical Simulation 19 (2018) 681–697.

[33] J. Leblond, J. Devaux, J. Devaux, Mathematical modelling of transformation plasticity in steels I: Case of ideal-plastic phases, International Journal of Plasticity 5 (1989) 551–572.

[34] J. B. Leblond, Mathematical modelling of transformation plasticity in steels II: Coupling with strain hardening phenomena, International Journal of Plasticity 5 (1989) 573–591.

[35] L. Taleb, F. Sidoroff, A micromechanical modeling of the Greenwood–Johnson mechanism in transformation induced plasticity, International Journal of Plasticity 19 (2003) 1821–1842.

[36] A. Ekberg, E. Kabo, H. Andersson, An engineering model for prediction of rolling contact fatigue of railway wheels, Fatigue <html_ent glyph="@amp;" ascii="&"/> Fracture of Engineering Materials and Structures 25 (2002) 899–909.

[37] K. A. Meyer, D. Nikas, J. Ahlström, Microstructure and mechanical properties of the running band in a pearlitic rail steel: Comparison between biaxially deformed steel and field samples, Wear 396-397 (2018) 12–21.

[38] A. S. Pandkar, N. Arakere, G. Subhash, Ratcheting-based microstructure-sensitive modeling of the cyclic hardening response of case-hardened bearing steels subject to Rolling Contact Fatigue, International Journal of Fatigue 73 (2015) 119–131.

[39] G. Schleinzer, F. Fischer, Residual stress formation during the roller straightening of railway rails, International Journal of Mechanical Sciences 43 (2001) 2281–2295.

[40] A. Al-Juboori, H. Zhu, D. Wexler, H. Li, C. Lu, A. McCusker, J. McLeod, S. Pannila, J. Barnes, Structural and microstrutural investigation of two distinct classes of white etching layer formation on the rail, in: 11th International Conference on Contact Mechanics and Wear of Rail/Whell Systems (CM2018), Delft, The Netherlands, 2018, p. 7.

[41] H. Zhu, H. Li, A. Al-Juboori, D. Wexler, C. Lu, A. McCusker, J. McLeod, S. Pannila, J. Barnes, Understanding and treatment of squat defects in a railway network, Wear 442-443 (2020) 203139.

[42] O. Vargolici, P. Merino, A. Saulot, J. Cavoret, S. Simon, F. Ville, Y. Berthier, Influence of the initial surface state of bodies in contact on the formation of white etching layers under dry sliding conditions, Wear 366-367 (2016) 209–216.

[43] B. Steel, Rail steel grades, https://britishsteel.co.uk/media/40810/steel-grade-dimensions-and-properties.pdf, ????

[44] D. Rittel, G. Ravichandran, A. Venkert, The mechanical response of pure iron at high strain rates under dominant shear, Materials Science and Engineering: A 432 (2006) 191–201.

[45] M. Sebès, L. Chevalier, J.-B. Ayasse, H. Chollet, A fast-simplified wheel–rail contact model consistent with perfect plastic materials, Vehicle System Dynamics 50 (2012) 1453–1471.

[46] P. Aknin, J. Pascal, J. Bettembourg, B. Prasil, Contribution of railway dynamics codes to the understanding of the metallurgical behavior of the rail tread, Wear 191 (1996) 126–132.

[47] M. Ishida, T. Moto, M. Takikawa, The effect of lateral creepage force on rail corrugation on low rail at sharp curves, Wear 253 (2002) 172–177.

[48] Z. Li, X. Zhao, R. Dollevoet, M. Molodova, Differential wear and plastic deformation as causes of squat at track local stiffness change combined with other track short defects, Vehicle System Dynamics 46 (2008) 237–246.

[49] Z. Li, X. Zhao, C. Esveld, R. Dollevoet, M. Molodova, An investigation into the causes of squats—Correlation analysis and numerical modeling, Wear 265 (2008) 1349–1355.

[50] E. Wild, L. Wang, B. Hasse, T. Wroblewski, G. Goerigk, A. Pyzalla, Microstructure alterations at the surface of a heavily corrugated rail with strong ripple formation, Wear 254 (2003) 876–883.

[51] M. Busquet, L. Baillet, C. Bordreuil, Y. Berthier, 3D finite element investigation on the plastic flows of rolling contacts—correlation with railhead microstructural observations, Wear 258 (2005) 1071–1080.

[52] M. Ishida, N. Abe, Experimental study on rolling contact fatigue from the aspect of residual stress, Wear 191 (1996) 65–71.

[53] K. Johnson, The Mechanics of Plastic Deformation of Surface and Subsurface Layers in Rolling And Sliding Contact, Key Engineering Materials 33 (1991) 17–34.

[54] K. Kondo, K. Yoroizaka, Y. Sato, Cause, increase, diagnosis, countermeasures and elimination of Shinkansen shelling, Wear 191 (1996) 199–203.

[55] M. Ertz, K. Knothe, Thermal stresses and shakedown in wheel/rail contact, Archive of Applied Mechanics (Ingenieur Archiv) 72 (2003) 715–729.

[56] J. Chaboche, Constitutive equations for cyclic plasticity and cyclic viscoplasticity, International Journal of Plasticity 5 (1989) 247–302.